Spectrochimica Acta Part B 111 (2015) 8–14

Contents lists available at ScienceDirect

Spectrochimica Acta Part B

journal homepage: www.elsevier.com/locate/sab

Calibration-free analysis of immersed brass alloys using long-ns-duration pulse laser-induced breakdown spectroscopy with and without correction for nonstoichiometric ablation

Tomoko Takahashi [a,*], Blair Thornton [a], Koichi Ohki [b], Tetsuo Sakka [c]

[a] Institute of Industrial Science, The University of Tokyo, Komaba, Meguro-ku, Tokyo 153-8505, Japan
[b] OK Lab. Co., Ltd. 8-7-3 Shimorenjyaku, Mitaka, Tokyo 181-0013, Japan
[c] Department of Energy and Hydrocarbon Chemistry, Graduate School of Engineering, Kyoto University, Nishikyo-ku, Kyoto 615-8510, Japan

ARTICLE INFO

Article history:
Received 21 July 2014
Accepted 13 June 2015
Available online 20 June 2015

Keywords:
Laser-induced breakdown spectroscopy (LIBS)
Calibration-free LIBS
Liquid-phase laser ablation
Quantitative analysis
Long-pulse laser

ABSTRACT

Long-ns-duration, single pulse laser-induced breakdown spectroscopy (LIBS) is known to be an effective method to observe well resolved spectra from samples immersed in water at high hydrostatic pressures. The aim of this study is to investigate whether the signals obtained using this method are suitable for quantitative analysis of chemical composition. Six certified brass alloys consisting of copper (Cu), zinc (Zn) and lead (Pb) were measured underwater using a laser pulse of duration 250 ns, and their compositions were determined using calibration-free LIBS (CF-LIBS) and corrected CF-LIBS (CCF-LIBS) methods. The mass fractions of Cu and Zn calculated using CF-LIBS showed better agreement with the certified values than those determined using CCF-LIBS, with relative errors of Cu 4.2 ± 3.3 % and Zn 7.2 ± 6.4 %. From the results, it can be said that the difference of preferential evaporation and ablation among elements does not need to be considered for underwater measurements with the long-pulse LIBS setup used in this work. While the results indicate that the CF-LIBS method can be applied for in situ quantitative analysis of major elements with concentrations > ~10 %, the mass fractions determined for Pb, with concentrations < 5 % had large relative errors, suggesting that an alternative method is required to quantify minor elements.

1. Introduction

Laser-induced breakdown spectroscopy (LIBS) is a form of atomic emission spectroscopy that analyzes the light emitted from atoms and ions of ablated material in a plasma created by a high intensity laser pulse. The excited atoms and ions emit specific wavelengths of light as they relax back to their ground state, which allows for simultaneous multi-element detection. LIBS is a promising tool for on-site chemical analysis and has been applied to the surveys of nuclear powers plants [1,2], planetary [3,4] and deep-sea explorations [5–7]. However, LIBS signals obtained underwater using a conventional single pulse method are significantly degraded compared to measurements in gaseous environments [8–10]. While it is well documented that the quality of the signals can be improved using a double-pulse method, in which two laser pulses are fired successively to generate a plasma in a cavitation bubble [11], it has been reported that the signal enhancement reduces at high hydrostatic pressures [12–14], with no enhancement seen beyond 14.6 MPa (146 atm.) for immersed solids [12]. Meanwhile, it has also been demonstrated that the use of a long-duration pulse > 100 ns can yield significant enhancements in signal quality for underwater samples [15,16]. It has further been shown that well resolved spectra can be observed for both bulk liquids [17] and submerged solids [18] at pressures of up to 30 MPa with little effect of external pressure using a long-pulse technique. This method has been applied to in situ measurements of seawater and hydrothermal deposits at depths of more than 1000 m, using a 3000 m depth rated long-pulse LIBS device, ChemiCam [5]. The aim of this study is to investigate whether the signals obtained using the long-pulse technique are suitable for quantitative analysis.

Conventional methods to quantify the chemical composition of samples require matrix matched standards, since the signals observed using atomic emission spectroscopy are matrix dependent [19–21]. In order to develop a more general method for quantification, calibration-free LIBS (CF-LIBS) has been introduced to determine chemical composition without the need for calibration curves, by accounting for matrix effects theoretically through analysis of the spectrum [22]. While CF-LIBS has been shown to be effective for quantification of compositions of samples in a gaseous environment, its application to long-pulse measurements of immersed samples needs further investigation. In ref. [23] it was reported that the atomic Cu/Zn ratio of species in the light emitting region of the plasma is significantly lower than the ratio of the immersed target when using a long pulse. It was suggested that for the experimental

* Corresponding author. Tel./fax: +81 3 5452 6489.
E-mail address: takahas@iis.u-tokyo.ac.jp (T. Takahashi).

http://dx.doi.org/10.1016/j.sab.2015.06.009

setup used, the condition of stoichiometric ablation, an underlying assumption of the CF-LIBS method, was not satisfied. While the stoichiometric ablation of brass is observed at low pressure in an argon gas environment [24], a similar discrepancy between values calculated by CF-LIBS and the actual composition has also been reported for experiments in air using a conventional duration ns single pulse [25,26]. Lednev et al. [25] suggested a Corrected CF-LIBS (CCF-LIBS) approach in which the preferential evaporation of a specific element due to nonstoichiometric ablation is taken into account in the calculation. In this study, we compare the results of calculations using CF-LIBS and CCF-LIBS for six certified brass alloys immersed in pure water at atmospheric pressure, and investigate which of the techniques is more suitable for in situ quantitative analysis with the long-pulse setup used in this work.

2. Experimental setup

The experimental setup used in this work is shown in Fig. 1. The laser pulse is generated using a custom-made 1064 nm Nd:YAG Q-switched laser that delivers a single 5 mJ pulse of duration 250 ns via a 600 μm fused-silica fiber at a repetition rate of 1 Hz. The laser pulse is focused onto a target in pure water 4 mm away from the face of a Cassegrain reflection optic of 5× magnification. The diameter of the laser beam at its focal point is 120 μm. The observed light passes through a custom-built spectrograph and the spectra are recorded using an intensified charge-coupled device (ICCD, Princeton Instruments, PiMAX 3 Gen II) from 250 nm to 570 nm with a resolution of ~0.8 nm. The wavelength and intensity calibrations were performed using a standard mercury (Ocean Optics, HG-1) and deuterium-halogen (Ocean Optics, DH-2000-CAL) light source, respectively. The gate width and the gate delay of the ICCD were set to 500 ns and 800 ns respectively, as these values were optimized to achieve the largest signal-to-noise ratio (SNR) through preliminary experiments using the setup.

Six brass certified reference materials (MBH Analytical Ltd.); a) 31X7835.5, b) 31XB23, c) 31X7835.8, d) 31XB21, e) 31XB20, and f) 31XB2 were used as targets in the experiments. The six samples have different mass fractions of Cu, Zn and Pb, as shown in Table 1. The target surfaces were observed using a microscope (Keyence, VK-9700) and show visible grain boundaries for some of the samples (see Fig. 2) and so the irradiation point was moved every 20 measurements in order to limit the effects of local inhomogeneity and allow for more representative characterization of the samples.

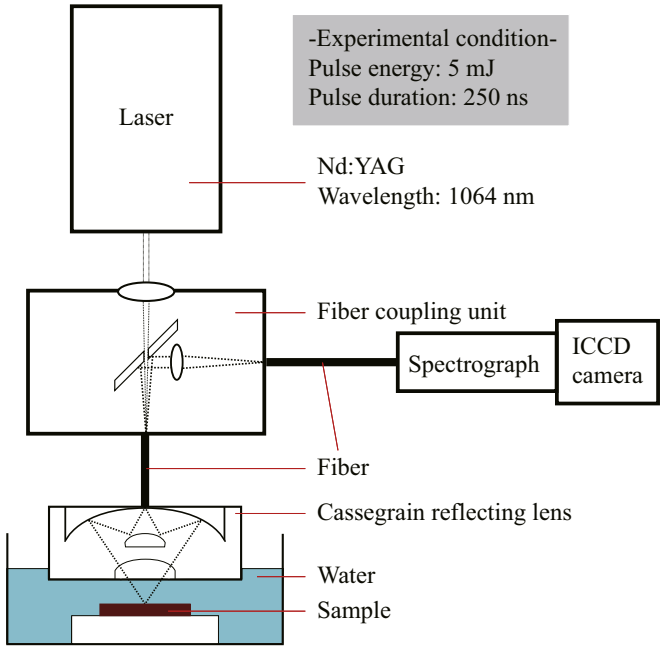

Fig. 1. Experimental setup.

3. Signal processing

3.1. CF-LIBS approach

Here we introduce the basic outline of CF-LIBS calculations. A more detailed description of the method can be found in refs. [20,22,27]. The main assumptions of CF-LIBS are that the following conditions are satisfied; local thermal equilibrium (LTE), absence of self-absorption and the stoichiometric ablation. The electron densities for the experiments carried out in this work are in the order of several 10^{16} (cm^{-3}), two orders of magnitude higher than the lowest limit of the electron densities, satisfying the McWhirter criterion [27–30]. It has been recently reported that the McWhirter criterion alone is not sufficient to conclude that LTE conditions are satisfied [19,31], and that additional measurements are necessary. While the additional measurements were not made in this work, the diffusion lengths and the relaxation times are calculated for the Cu, Pb, and Zn peaks used in this work by applying the equations in ref. [19]. The calculated diffusion lengths are in the order of several 10 μm, 1 ~ 10 μm and 1 ~ 10 μm respectively, all of which are much smaller than the size of the plasma being observed which is several 100 μm [18]. The calculated relaxation times are in the order of several 10 ns, 1 ~ 10 ns and 1 ~ 10 ns respectively. These relaxation times are considered to be significantly shorter than the overall plasma extinction time, and so we assume that the LTE conditions are warranted in the timescale used in this work. The effect of self-absorption is discussed in Sect. 4.

The assumption of stoichiometric ablation is investigated experimentally through comparison of the Cu, Zn and Pb mass fractions determined for the six samples using CF- and CCF-LIBS with their certified values.

3.1.1. Plasma temperature

The excitation temperature (hereafter temperature) is calculated based on the spectral lines of a single element using the Boltzmann distribution law,

$$\frac{\ln I_{s\_ij}}{A_{s\_ij} g_{s\_i}} = -\frac{E_{s\_i}}{k_B T} + \ln\left(\frac{FN_s}{U_s(T)}\right), \tag{1}$$

where I_{s_ij} is the intensity of the spectral line in arbitrary units, A_{s_ij} is the transition probability (s^{-1}), g_{s_i} is the statistical weight, E_{s_i} is the excitation energy (eV), k_B is the Boltzmann constant (eV K^{-1}), T is the temperature (K), F is an experimental parameter, N_s is the number density of each emitted species and $U_s(T)$ is the partition function. The subscripts i, j and s indicate the upper energy level i and lower energy level j of the element s. The parameters A_{s_ij}, g_{s_i}, E_{s_i} and $U_s(T)$ are obtained from the National Institute of Standards and Technology (NIST) database [32] and Kurucz atomic spectral line database [33]. When a single element is considered, the values of $-1/k_BT$ and $\ln(FN_s/U_s(T))$ in Eq. (1) are constant. When $\ln(I_{s\_ij}/A_{s\_ij} g_{s\_i})$ is plotted against E_{s_i} for more than two transition lines, a linear Boltzmann plot can be obtained [20]. The temperature T can be determined from the slope of the Boltzmann plot, i.e. $-1/k_BT$.

3.1.2. Electron number density

Since no ionic lines are seen for the underwater samples measured in this work over the observed spectral range, the electron number density was determined from the Stark broadening effect [19] using the following simplified relation:

$$\Delta\lambda_{1/2} \approx \frac{2wN_e}{10^{16}}, \tag{2}$$

Table 1
Mass fractions of Cu, Zn, and Pb in the certified samples.

Sample	a) 31X7835.5		b) 31XB23		c) 31X7835.8		d) 31XB21		e) 31XB20		f) 31XB2	
	Conc. (%)	Unc. (%)	Conc. (%)	Unc. (%)	Conc. (%)	Unc. (%)	Conc. (%)	Unc. (%)	Conc. (%)	Unc. (%)	Conc. (%)	Unc. (%)
Cu	91.25	0.12	89.57	0.06	69.93	0.12	69.24	0.12	58.53	0.1	60.13	0.1
Zn	6.23	0.06	9.97	0.06	24.83	0.06	29.5	0.14	37.03	0.17	39.57	0.12
Pb	1.64	0.04	0.046	0.002	3.15	0.03	0.12	0.004	4.43	0.06	0.0129	0.0014
Others	0.88	-	0.41	-	2.09	-	1.14	-	0.01	-	0.29	-

where $\Delta\lambda_{1/2}$ is the full width at half maximum (FWHM) of Stark broadened lines (nm), w is the electron impact width parameter and N_e is the electron number density. The value of w was obtained from ref. [34]. The resolution of the instrument is taken into account as follows:

$$\Delta\lambda_{1/2} = \Delta\lambda_{observed} - \Delta\lambda_{instrument}, \tag{3}$$

where the instrument width $\Delta\lambda_{instrument}$ is determined as 0.9 nm using the line width of the Hg line observed at 435.8 nm during wavelength calibration. It should be noted that Eq. (3) is valid if both Stark and instrumental profiles are considered as Lorentzian functions [19]. For the sake of simplicity, we assumed that each spectral line to be observed as a Lorentzian profile in this work [23,35].

3.1.3. Estimation of elemental composition

Once T is obtained, N_s of all the elements seen as spectral lines in the spectrum can be calculated using Eq. (1). Since only the neutral atomic species are observed over the spectral range used in this work, the number densities of the single ionized species are calculated using the Saha equation [19]:

$$N_e \frac{N_s^{II}}{N_s^{I}} = \frac{(2\pi m_e k_B T)^{3/2}}{h^3} \frac{2U_s^{II}(T)}{U_s^{I}(T)} e^{-E_{s\_ion}/k_B T}, \tag{4}$$

where N_s^I and N_s^{II} are the number densities of the neutral atomic species and the single ionized species (cm^{-3}), respectively. E_{s_ion} is the ionization potential of each neutral species in its ground state (eV), m_e is the electron mass (eV m^2 s^{-2}), and h is Planck's constant (eV K^{-1}). T and N_e are calculated as described in Sect. 3.1.1 and 3.1.2, respectively. The total number density of each species (N_s^{tot}) is determined by adding number densities of the neutral atomic species and single ionized species,

$$N_s^{tot} = N_s^{I} + N_s^{II} \tag{5}$$

Finally, the mass concentration of each species, C_s^{CF}, is defined as follows:

$$C_s^{CF} = \frac{m_s N_s^{tot}}{\sum_s^n m_s N_s^{tot}}, \tag{6}$$

where m_s is the atomic weight of the sth element and n is the total number of elements observed in the target.

3.2. CCF-LIBS approach

In the CF-LIBS method, the mass fraction of element s in the plasma is calculated as C_s^{CF}. While C_s^{CF} indicates the mass fraction of an element in the plasma, if nonstoichiometric ablation occurs, the mass fraction of an element in the plasma region is not the same as that in the target. In CCF-LIBS, the work function W is introduced to compensate for this effect [25],

$$\frac{C_s^{CCF}}{C_{s'}^{CCF}} = \frac{C_s^{CF} W_s}{C_{s'}^{CF} W_{s'}}, \tag{7}$$

where C_s^{CCF} indicates the mass fraction of the element s and s' indicates an element other than s. W_s is defined by the following equation,

$$W_s = (c_{s\_solid}(T_{s\_melt} - T_{room}) + \Delta H_{s\_fusion} + c_{s\_liquid}(T_{s\_evap} - T_{s\_melt}) + \Delta H_{s\_evap}) T_{s\_melt}, \tag{8}$$

where c_{s_solid} is the heat capacity in the solid state (J mol^{-1} K^{-1}), T_{s_melt} is the melting temperature (K), T_{room} is the room temperature (K), ΔH_{s_fusion}

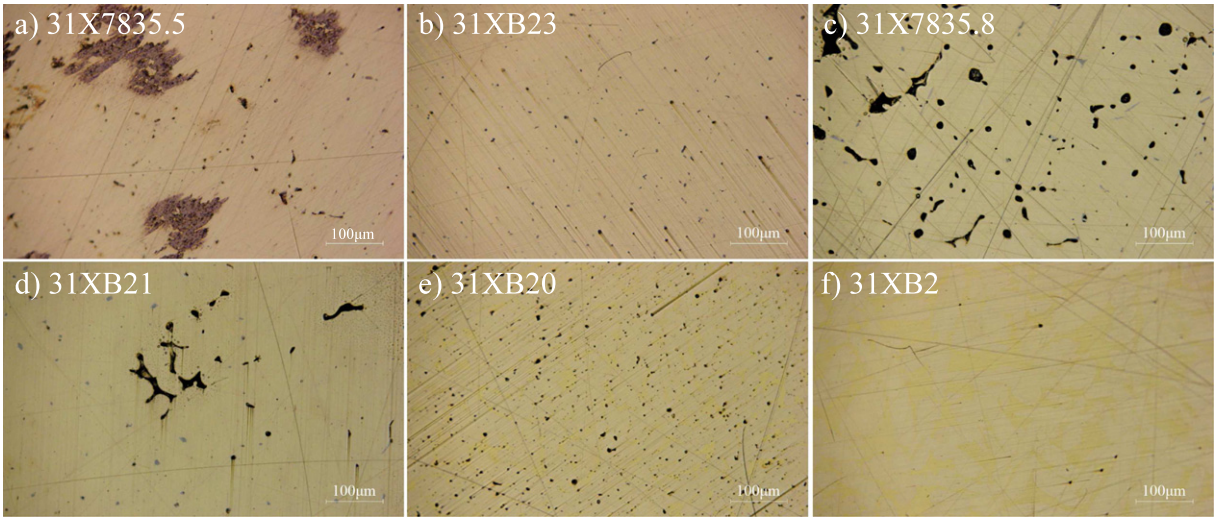

Fig. 2. Images of the surface of brass samples taken at a magnification of 20×. The black spots and lines are stains and scratches. The local changes of color, which are thought to be grain boundaries, are observed in the images of a) 31X7835.5, e) 31XB20 and f) 31XB2.

Table 2
Thermal and optical properties of Cu, Zn and Pb used in the calculation of the work function W, where values are taken from refs. [36,37].

	c_{solid}	T_{melt}	ΔH_{fusion}	c_{fluid}	T_{boil}	ΔH_{evap}	$W \times 10^{-8}$
	($J\ mol^{-1}K^{-1}$)	(K)	($kJ\ mol^{-1}$)	($J\ mol^{-1}\ K^{-1}$)	(K)	($kJ\ mol^{-1}$)	($J\ K\ mol^{-1}$)
Cu	24.44	1358	13.3	30.5	2835	300	5.22
Zn	25.39	692.7	7.07	32.3	1180	190	1.54
Pb	26.84	600.6	4.77	29.4	2022	180	1.41

is the enthalpy of melting ($J\ mol^{-1}$), c_{s_liquid} is the heat capacity in the liquid state ($J\ mol^{-1}\ K^{-1}$), T_{s_evap} is the temperature of evaporation (K) and ΔH_{s_evap} is the enthalpy of evaporation ($J\ mol^{-1}$). Table 2 shows the parameters for the calculation of W_s used in the CCF-LIBS approach. The thermal and optical properties were obtained from refs. [36,37]. For this study, T_{room} is the water temperature which is set to be 25 °C. All other steps of the calculation are the same as for CF-LIBS.

4. Results and discussion

The spectra obtained from the submerged samples are shown in Fig. 3. The background is subtracted and the spectra are normalized to have a maximum intensity of 1. The spectral lines of Cu I at 324.8, 327.4, 510.6, 515.3 and 521.8 nm, Zn I at 334.5, 472.2 and 481.1 nm and Pb I at 405.8 nm are visible in all the spectra. In spectra c), d), e), and f), the lines of Zn I at 468.0 nm are seen. The ratio of Zn/Cu of the samples increases from sample a) to f), which is clearly visible from the relative intensities of the Zn I and Cu I spectral lines in the spectra. Other spectral lines of Pb I, at 364.0 and 368.3 nm, can be also seen in the spectra of samples a), c) and e), which have the Pb mass fractions > 1%. These spectral lines could not be detected in the spectra of the samples b), d) and f), where the mass fractions are < 1% Pb.

Table 3
Wavelength λ, the transition probability A_{s_ij}, the upper level energy E_{s_i}, and the statistical weight g_{s_i} of atomic lines of Cu, Zn and Pb used in the CF-LIBS calculation. The wavelength and other data were obtained from [32] and [33], respectively.

	λ	A_{s_ij}	E_{s_i}	g_{s_i}
	(nm)	($10^8\ s^{-1}$)	(eV)	
Cu I	510.6	0.0195	3.82	4
Cu I	515.3	1.03	6.19	4
Cu I	521.8	1.22	6.19	6
Zn I	481.1	0.700	6.65	3
Pb I	405.8	0.912	4.38	3

The spectral lines which are clearly visible without the self-reversal in all the spectra are used for the calculation of CF- and CCF-LIBS. Other lines where lower energy levels of the transition are the ground state were not used because it is reported that they often have serious self-absorption [38]. It should be noted that the absence of self-reversal in peaks is not a sufficient condition that the peaks are not affected by the self-absorption [19]. In order to evaluate the effects of self-absorption, the integral intensity ratios of the peaks were calculated. While the integral intensity ratio of the peaks of Cu I at 327.4 to

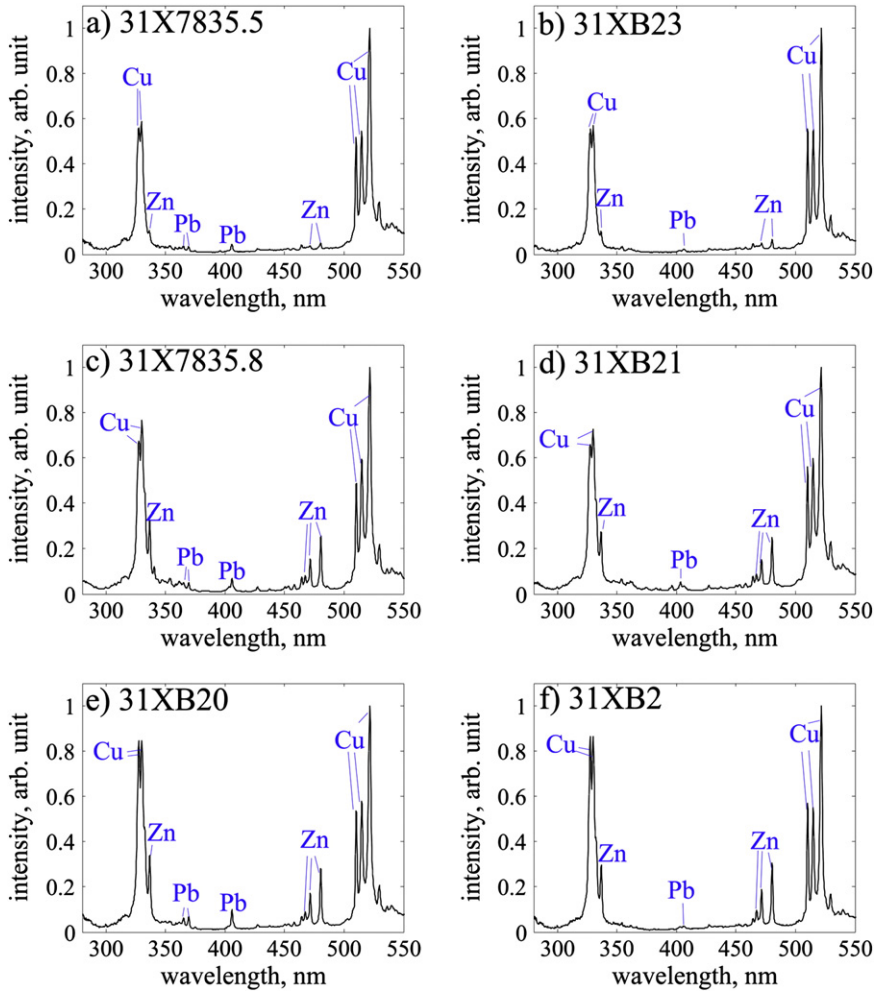

Fig. 3. Spectra of the six brass targets obtained underwater using long-pulse LIBS. The elements corresponding to each emission line are written above each identified spectral line.

Table 4
Temperature and electron number density calculated using Eq. (1) and (2) respectively.

Sample	T emperature (K)	Electron density (cm^{-3})
a) 31X7835.5	7750 ± 750	$2.79 \pm 0.41 \times 10^{16}$
b) 31XB23	7350 ± 850	$2.56 \pm 0.42 \times 10^{16}$
c) 31X7835.8	7350 ± 810	$2.34 \pm 0.16 \times 10^{16}$
d) 31XB21	8230 ± 720	$2.45 \pm 0.13 \times 10^{16}$
e) 31XB20	7480 ± 1050	$2.34 \pm 0.24 \times 10^{16}$
f) 31XB2	7320 ± 930	$2.32 \pm 0.24 \times 10^{16}$

324.8 nm, whose lower energy levels are the ground state, is calculated to be ~1.2, which is much smaller than the theoretical ratio of 2, the intensity ratio of Cu I at 521.8 to 515.3 nm is calculated to be ~2, which is close to the theoretical value of 1.8, indicating that the effects of self-absorption are small.

The CF- and CCF-LIBS algorithms were implemented in Matlab (Mathwork Inc.). The spectral line area was used as the input value for the spectral line intensity in Eq. (1), as this was found to be more robust to noise than the maximum intensity. The spectral line was modeled using a Lorentzian curve fit [23] and its area was calculated by integrating the area under the Lorentzian curve after removing the continuum light. The three spectral lines of Cu I at 510.6, 515.3 and 521.8 nm overlap due to broadening, and were modeled using multiple Lorentzian curves. For the samples studied, we assume that the targets contain only Cu, Zn and Pb since the mass fractions of other minor elements in the targets, such as Sn, are only at trace levels. Spectral lines at low intensity and those that overlap significantly with adjacent spectral lines were rejected. The parameters of spectral lines used in the final calculation are summarized in Table 3. The electron density was calculated with the data of a Zn I spectral line at 481.1 nm, since the line was well resolved from the adjacent lines in all the observed spectra. The temperature was calculated with the data of Cu I spectral lines at 510.6, 515.3 and 521.8 nm. For the calculation of temperature, spectral lines with more than two different upper energy levels need to be clearly observable, and only Cu I fulfills this condition with the setup used in this study. The temperature and the electron density calculated are shown in Table 4. The temperatures were calculated to be within 7500 K ± 1500 K for all the samples. 300 spectra were obtained for each sample, and outliers were removed using the Smirnov-Grubbs rejection test [39]. The difference between the spectra observed by first and other shots was not considered since it is negligible with our experimental setup. This is due to the small amount of material ablated when using a long pulse [40]. Should there be a large difference in the spectra of the first and subsequent shots, the spectra would be rejected by the test. Approximately 90 % of the spectra satisfied the Smirnov-Grubbs rejection test, and 30 spectra were randomly selected for the CF- and CCF-LIBS analysis without accumulation of the intensities of the spectra. Since our motive is to apply LIBS to an in situ measurement in a deep-sea environment, 30 spectra is considered as a reasonable number of measurements for each target at a repetition rate of 1 Hz used in our system. The results of CF- and CCF-LIBS of the different brass targets are shown in Fig. 4 and Table 5, where the values shown are the average of the 30 measurements and the error bars represent the standard deviation. From the results, it is clear that the composition is more accurately represented by the CF-LIBS calculation than the CCF-LIBS calculation for all six samples. In particular, the actual values of Cu and Zn are within the range of the standard deviations of the calculated values using CF-LIBS for all six samples, with relative errors of Cu 4.2 ± 3.3% and Zn 7.2 ± 6.4%. The values calculated using CCF-LIBS were found to consistently overestimate Cu and underestimate Zn, and, for the experimental setup used in this work, were not found to be representative of actual composition. The fact that $W_{Cu} > W_{Zn}$ or W_{Pb} implies that CCF-LIBS will always estimate the Zn/Cu and Pb/Cu ratios less than CF-LIBS. On average, the values of Cu and Zn calculated using CF-LIBS agree to within 10% of the certified values, and it can be said that the difference of preferential evaporation and ablation among elements does not need to be considered for the underwater measurement with the long-pulse LIBS setup used in this study. Although it has been reported that fractionation of Cu might disturb stoichiometric ablation [41–43], since the Cu values determined in this work are not consistently smaller than their certified values, as would be expected if fractionation played a significant role in perturbing the results, it can be said that the effects of fractionation are at most in the same order as other sources of uncertainty for the experimental setup used. Meanwhile, previous research performed underwater using a long pulse of similar pulse energies reported nonstoichiometric atomization at the periphery of the plume [23]. One possible reason why the compositions could be calculated using CF-LIBS without correction of preferential evaporation may be

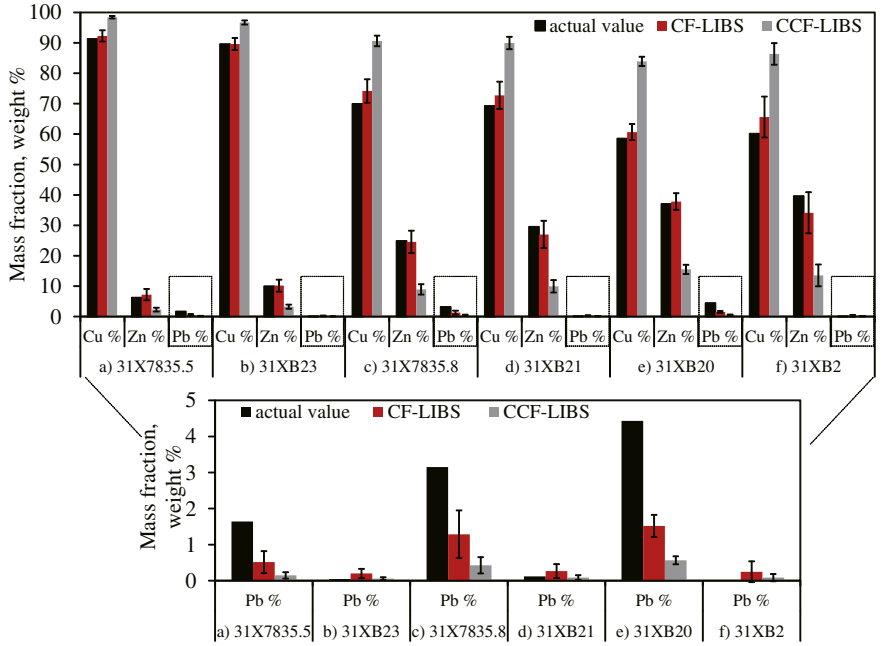

Fig. 4. Results of calculation using the CF-LIBS method. The subfigure at the bottom shows the enlargement of the Pb mass fraction.

Table 5
Relative errors (R. E.) and the absolute errors (A. E.) of compositions calculated using the CF- and CCF-LIBS methods.

Sample		Cu	R. E.	A. E.	Zn	R. E.	A. E.	Pb	R. E.	A. E.
		(%)	(%)	(%)	(%)	(%)	(%)	(%)	(%)	(%)
a) 31X7835.5	CF	92 ± 2	1	1	7.2 ± 1.9	16	1.0	0.52 ± 0.31	69	-1.1
	CCF	98 ± 1	8	7	2.4 ± 0.6	63	-3.9	0.12 ± 0.07	91	-1.5
b) 31XB23	CF	90 ± 2	0	0	10 ± 2	2	0	0.20 ± 0.13	336	0.15
	CCF	97 ± 1	8	7	3.3 ± 0.7	67	-6.7	0.058 ± 0.038	27	0.012
c) 31X7835.8	CF	74 ± 4	6	4	25 ± 4	1	0	1.3 ± 0.7	59	-1.9
	CCF	91 ± 2	30	21	8.9 ± 1.7	64	-16	0.43 ± 0.22	86	-2.7
d)31XB21	CF	73 ± 4	5	4	27 ± 5	8	-3	0.27 ± 0.19	124	0.15
	CCF	90 ± 2	30	21	10 ± 2	66	-20	0.090 ± 0.064	25	-0.030
e) 31XB20	CF	61 ± 3	4	2	38 ± 3	2	1	1.5 ± 0.3	66	-2.9
	CCF	84 ± 2	43	25	16 ± 2	58	-22	0.57 ± 0.11	87	-3.9
f) 31XB2	CF	66 ± 7	9	5	34 ± 7	14	-5	0.20 ± 0.29	1824	0.24
	CCF	86 ± 4	44	26	14 ± 4	66	-26	0.088 ± 0.100	579	0.075

related to the fact that the laser was irradiated through a fiber optic cable in this work, which makes the laser beam profile a relatively homogenous top-hat shape, while a lens was used for irradiation of the laser in the previous research. In our future work, the relation between the power density, beam profile and the calculated results of CF-LIBS will be examined to further investigate this point.

While the mass fractions of Cu and Zn calculated in this work have relative errors averaging < 10%, the mass fractions determined for Pb are relatively large. This may be partially due to the fact that the spectral line of Pb is too small to calculate its area accurately, considering that these four samples contain less than 2% of Pb. While the average SNR of peak heights of Cu I and Zn I are 30 ~ 70 and 5 ~ 20 respectively, the SNR of Pb I at 405.8 nm for samples a), b), d) and f) were 1.7 ~ 2.6, which might be too small for peak detection. Although for samples c) and e) the SNR are 4.7 and 6.4 respectively, which may be large enough for peak detection, Pb mass fractions were underestimated with large relative errors. Since the mass fraction of one element calculated using CF- and CCF-LIBS is influenced by the calculated abundance of the other elements, the absolute errors in the calculation of the major constituting elements directly affect the absolute errors of the minor constituting elements, resulting in large relative errors of minor elements. It should be noted, however, that some works performed in air have successfully determined the compositions of metal samples including minor constituting elements with small absolute and relative errors [30,44]. Compared to those obtained in measurements in air, since the spectral lines tend to be broadened in underwater measurement, larger errors in the calculation in this work might occur in the calculation of spectral line areas. This suggests that improved algorithms for spectral line separation and calculation of spectral line area need to be developed in future works. However, the fact that the errors are non-separable and so not independent poses an inherent problem for calibration-free methods for quantifying the concentration of minor elements. It is suggested that for underwater measurements using long-pulse LIBS, the application of CF-LIBS calculations should be limited to the major constituents, and alternative methods with separable errors between elements, such as matrix matched calibration curves, should be used to quantify minor constituting elements.

5. Conclusion

Quantitative analysis of brass targets submerged in pure water has been investigated using two calibration-free based methods, CF-LIBS and CCF-LIBS. The results demonstrate that the CF-LIBS method determined the mass fractions of major elements with concentrations > 10%, which in this case are Cu and Zn, with relative errors of less than 10%. From the results, it can be said that, considering Cu and Zn, preferential evaporation and ablation among major elements does not have a significant influence on the quantification of the submerged metallic samples investigated with the long pulse setup used in this study. The results suggest that CF-LIBS can be potentially applied for in situ quantification of water-immersed brass alloys measured using a single long pulse. However, while the application of CF-LIBS is adequate to quantify concentrations of major elements, the mass fractions of Pb, with concentrations < 5%, could not be reliably determined. The main reason for this is thought to be due to the inherently inseparable nature of the estimation errors characteristic to calibration-free methods. Alternative methods should be investigated to improve the estimates of minor element mass fractions for underwater measurements using a long-ns-duration pulse.

Acknowledgment

This project is funded by the Japanese Ministry of Education under the 'Program for the development of fundamental tools for the utilization of marine resources'.

References

[1] M. Saeki, A. Iwanabe, C. Ito, I. Wakaida, B. Thornton, T. Sakka, H. Ohba, Development of a fiber-coupled laser-induced breakdown spectroscopy instrument for analysis of underwater debris in a nuclear reactor core, J. Nucl. Sci. Technol. 51 (2014) 930–938.
[2] A.I. Whitehouse, J. Young, I.M. Botheroyd, S. Lawson, C.P. Evans, J. Wright, Remote material analysis of nuclear power station steam generator tubes by laser-induced breakdown spectroscopy, Spectrochim. Acta Part B 56 (2001) 821–830.
[3] B. Sallé, J.-L. Lacour, P. Mauchien, P. Fichet, S. Maurice, G. Manhès, Comparative study of different methodologies for quantitative rock analysis by laser-induced breakdown spectroscopy in a simulated Martian atmosphere, Spectrochim. Acta Part B 61 (2006) 301–313.
[4] P.-Y. Meslin, O. Gasnault, O. Forni, et al., Soil diversity and hydration as observed by ChemCam at Gale crater, Mars, Science 341 (2013) (1238670-1-10).
[5] B. Thornton, T. Takahashi, T. Sato, T. Sakka, A. Tamura, A. Matsumoto, T. Nozaki, T. Ohki, K. Ohki, Development of a deep-sea laser-induced breakdown spectrometer for in situ multi-element chemical analysis, Deep-Sea Res. I 95 (2015) 20–36.
[6] B. Thornton, T. Masamura, T. Takahashi, T. Ura, K. Ohki, T. Sakka, Development and field testing of laser-induced breakdown spectroscopy for in situ multi-element analysis at sea, Proc. IEEE Oceans'12, Hampton Roads, the U.S., 2012.
[7] B. Thornton, T. Ura, Effects of pressure on the optical emissions observed from solids immersed in water using a single pulse laser, Appl. Phys. Express 4 (2011) 022702.
[8] A. De Giacomo, M. Dell'Aglio, F. Colao, R. Fantoni, Double pulse laser produced plasma on metallic target in seawater: basic aspects and analytical approach, Spectrochim. Acta Part B 59 (2004) 1431–1438.
[9] V. Lazic, F. Colao, R. Fantoni, V. Spizzicchino, Recognition of archeological materials underwater by laser induced breakdown spectroscopy, Spectrochim. Acta Part B 60 (2005) 1014–1024.
[10] A.E. Pichahchy, D.A. Cremers, M.J. Ferris, Elemental analysis of metals under water using laser-induced breakdown spectroscopy, Spectrochim. Acta Part B 52 (1997) 25–39.
[11] R. Nyga, W. Neu, Double-pulse technique for optical emission spectroscopy of ablation plasmas of samples in liquids, Opt. Lett. 18 (1993) 747–749.
[12] A. De Giacomo, A. De Bonis, M. Dell'Aglio, O. De Pascale, R. Gaudiuso, S. Orlando, A. Santagata, G.S. Senesi, F. Taccogna, R. Teghil, Laser ablation of graphite in water in a range of pressure from 1 to 146 atm using single and double pulse techniques for the production of carbon nanostructures, J. Phys. Chem. C 115 (2011) 5123–5130.
[13] T. Takahashi, B. Thornton, T. Ura, Investigation of influence of hydrostatic pressure on double-pulse laser-induced breakdown spectroscopy for detection of Cu and Zn in submerged solids, Appl. Phys. Express 6 (2013) 042403.

[14] B. Thornton, T. Takahashi, T. Ura, T. Sakka, Cavity formation and material ablation for single-pulse laser-ablated solids immersed in water at high pressure, Appl. Phys. Express 5 (2012) 102402.
[15] T. Sakka, H. Oguchi, S. Masai, K. Hirata, Y.H. Ogata, M. Saeki, H. Ohba, Use of a long-duration ns pulse for efficient emission of spectral lines from the laser ablation plume in water, Appl. Phys. Lett. 88 (2006) 061120.
[16] T. Sakka, A. Tamura, A. Matsumoto, K. Fukami, N. Nishi, B. Thornton, Effects of pulse width on nascent laser-induced bubbles for underwater laser-induced breakdown spectroscopy, Spectrochim. Acta Part B 97 (2014) 94–98.
[17] B. Thornton, T. Sakka, T. Masamura, A. Tamura, T. Takahashi, A. Matsumoto, Long-duration nano-second single pulse lasers for observation of spectra from bulk liquids at high hydrostatic pressures, Spectrochim. Acta Part B 97 (2014) 7–12.
[18] B. Thornton, T. Sakka, T. Takahashi, A. Tamura, T. Masamura, A. Matsumoto, Spectroscopic measurements of solids immersed in water at high pressure using a long-duration nanosecond laser pulse, Appl. Phys. Express 6 (2013) 082401.
[19] D.W. Hahn, N. Omenetto, Laser-induced breakdown spectroscopy (LIBS), Part I: Review of basic diagnostics and plasma-particle interactions: still-challenging issues within the analytical plasma community, Appl. Spectrosc. 64 (2010) 335A–366A.
[20] E. Tognoni, G. Cristoforetti, S. Legnaioli, V. Palleschi, Calibration-free laser-induced breakdown spectroscopy: State of the art, Spectrochim. Acta Part B 65 (2010) 1–14.
[21] A.S. Eppler, D.A. Cremers, D.D. Hickmott, M.J. Ferris, A.C. Koskelo, Matrix effects in the detection of Pb and Ba in soils using laser-induced breakdown spectroscopy, Appl. Spectrosc. 50 (1996) 1175–1181.
[22] A. Ciucci, M. Corsi, V. Palleschi, S. Rastelli, A. Salvetti, E. Tognoni, New procedure for quantitative elemental analysis by laser-induced plasma spectroscopy, Appl. Spectrosc. 53 (1999) 960–964.
[23] T. Sakka, H. Yamagata, H. Oguchi, K. Fukami, Y.H. Ogata, Emission spectroscopy of laser ablation plume: Composition analysis of a target in water, Appl. Surf. Sci. 255 (2009) 9576–9580.
[24] J. Hermann, L. Mercadier, E. Mothe, G. Socol, P. Alloncle, On the stoichiometry of mass transfer from solid to plasma during pulsed laser ablation of brass, Spectrochim. Acta Part B 65 (2010) 636–641.
[25] V.N. Lednev, S.M. Pershin, Plasma stoichiometry correction method in laser-induced breakdown spectroscopy, Laser Phys. 18 (2008) 850–854.
[26] L. Fornarini, F. Colao, R. Fantoni, V. Lazic, V. Spizzicchino, Calibration analysis of bronze samples by nanosecond laser induced breakdown spectroscopy: A theoretical and experimental approach, Spectrochim. Acta B 60 (2005) 1186–1201.
[27] S. Pandhija, A.K. Rai, In situ multielemental monitoring in coral skeleton by CF-LIBS, Appl. Phys. B 94 (2009) 545–552.
[28] R.H. Huddlestone, S.L. Leonard, Plasma diagnostic techniques, in: R.W.P. McWhirter (Ed.), Spectral Intensities, Academic Press, New York 1965, pp. 201–264.
[29] M. Hanif, M. Salik, M.A. Baig, Quantitative studies of copper plasma using laser induced breakdown spectroscopy, Opt. Laser Eng. 49 (2011) 1456–1461.
[30] M.L. Shah, A.K. Pulhani, G.P. Gupta, B.M. Suri, Quantitative elemental analysis of steel using calibration-free laser-induced breakdown spectroscopy, Appl. Opt. 51 (2012) 4612–4621.
[31] G. Cristoforetti, A. De Giacomo, M. Dell'Aglio, S. Legnaioli, E. Tognoni, V. Palleschi, N. Omenetto, Local thermodynamic equilibrium in laser-induced breakdown spectroscopy: Beyond the McWhirter criterion, Spectrochim. Acta B 65 (2010) 86–95.
[32] NIST Atomic Spectra Database (version 5), [Online](Available: http://physics.nist.gov/asd3) National Institute of Standards and Technology, Gaithersburg, MD, March 15, 2014.
[33] P.L. Smith, C. Heise, J.R. Esmond, R.L. Kurucz, Kurucz Atomic Line DatabaseAvailable: http://www.cfa.harvard.edu/amdata/ampdata/kurucz23/sekur.html ([2014, March 15]).
[34] M.S. Dimitrijevic, S. Sahal-Bréchot, Stark broadening of neutral zinc spectral lines, Astron. Astrophys., Suppl. Ser. 140 (1999) 193–196.
[35] N.M. Shaikh, B. Rashid, S. Hafeez, Y. Jamil, M.A. Baig, Measurement of electron density and temperature of a laser-induced zinc plasma, J. Phys. D. Appl. Phys. 39 (2006) 1384–1391.
[36] W.M. Haynes (Ed.), CRC handbook of chemistry and physics, 93rd ed.CRC press, Boca Raton 2012, p. 12 (Ch. 4, 6).
[37] D. Bleiner, Z. Chen, D. Autrique, A. Bogaerts, Role of laser-induced melting and vaporization of metals during ICP-MS and LIBS analysis, investigated with computer simulations and experiments, J. Anal. At. Spectrom. 21 (2006) 910–921.
[38] D.A. Cremers, L.J. Radziemski, Handbook of Laser-Induced Breakdown Spectroscopy, John Wiley & Sons Inc, England, 2006. 109.
[39] F.E. Grubbs, Procedures for detecting outlying observations in samples, Technometrics 11 (1969) 1–21.
[40] T. Sakka, H. Oguchi, S. Masai, Y.H. Ogata, Quasi nondestructive elemental analysis of solid surface in liquid by long-pulse laser ablation plume spectroscopy, Chem. Lett. 36 (2007) 508–509.
[41] A. De Giacomo, M. Dell'Aglio, A. Casavola, G. Colonna, O. De Pascale, M. Capitelli, Elemental chemical analysis of submerged targets by double-pulse laser-induced breakdown spectroscopy, Anal. Bioanal. Chem. 385 (2006) 303–311.
[42] A. De Giacomo, M. Dell'Aglio, O. De Pascale, M. Capitelli, From single pulse to double pulse ns-laser induced breakdown spectroscopy under water: Elemental analysis of aqueous solutions and submerged solid samples, Spectrochim. Acta B 62 (2007) 721–738.
[43] F. Colao, R. Fantoni, V. Lazic, L. Caneve, A. Giardini, V. Spizzichino, LIBS as a diagnostic tool during the laser cleaning of copper based alloys: experimental results, J. Anal. At. Spectrom. 19 (2004) 502–504.
[44] K.K. Herrera, E. Tognoni, N. Omenetto, B.W. Smith, J.D. Winefordner, Semi-quantitative analysis of metal alloys, brass and soil samples by calibration-free laser-induced breakdown spectroscopy: recent results and considerations, J. Anal. At. Spectrom. 24 (2009) 413–425.